3D-Printed Organic Conjugated Trimer for Visible-Light-Driven Photocatalytic Applications

Xiaojiao Yuan, Neus Sunyer-Pons, Aleix Terrado, José Luis León, Georges Hadziioannou, Eric Cloutet, Katherine Villa

3D-Printed Organic Conjugated Trimer for Visible-Light-Driven Photocatalytic Applications

Xiaojiao Yuan, [a] *Neus Sunyer-Pons,* [a] *Aleix Terrado,* [a] *José Luis León,* [a] Georges Hadziioannou,[b] Eric Cloutet,[b] *Katherine Villa** [a]

[a] Institute of Chemical Research of Catalonia (ICIQ), The Barcelona Institute of Science and Technology (BIST). Av. Països Catalans, 16, Tarragona E-43007, Spain.

[b] Laboratoire de Chimie des Polymères Organiques (LCPO-UMR 5629), Université de Bordeaux, Bordeaux INP, CNRS, F-33607 Pessac, France.

ABSTRACT

Small molecules organic semiconductors (SMOS) have emerged as a new class of photocatalysts that exhibit visible light absorption, tunable band gap, good dispersion, and solubility. However, the recovery and reusability of such SMOS in multiple photocatalytic reactions is challenging. In this work, we report a 3D-printed hierarchical porous structure based on an organic conjugated trimer (4,7-Bis(thieno[3,4-b] [1,4] dioxin-5-yl) benzo[c] [1,2,5] thiadiazol, EBE). Upon manufacturing, the photophysical and chemical properties of the organic semiconductor were maintained. Interestingly, the 3D-printed EBE photocatalyst showed a longer lifetime (11.7 ns) compared to the powder state EBE, indicating microenvironment effect of solvent (acetone) and better dispersion, as well as reduced intermolecular π-π stacking, resulting in improved separation of charge carriers. As a proof-of-concept, we evaluated the photocatalytic activity of the 3D-printed EBE catalyst for water treatment and hydrogen production under sun-like irradiation. The resulting degradation efficiencies and hydrogen generation rates were higher than the ones reported for the state-of-the-art 3D-printed photocatalytic structures based on inorganic semiconductors. The photocatalytic mechanism was further investigated, and the results suggested that hydroxyl radicals ($HO^{\bullet}$) are the main radicals responsible for the degradation of an organic pollutant. Besides, the reusability of the EBE-3D photocatalyst was demonstrated in up to 5 recycling uses. Overall, these results provide the great potential of a novel 3D-printed organic conjugated trimer for photocatalysis applications.

KEYWORDS: Organic semiconductors, Conjugated trimer, 3D-printing, Photocatalysis, Hydrogen generation

INTRODUCTION

Solar-driven photocatalysis has the potential to alleviate current environmental pollution and energy shortage by using a simple setup, water, sunlight, and efficient photocatalytic materials. Recently, organic π-conjugated polymers (CPs) have been widely investigated as promising alternatives to traditional inorganic semiconductors for photocatalysis, due to their tunable optoelectronic properties, low cost, and high chemical stability.[1-7] However, poor dispersion and solubility in reaction media limit their overall practical applications.

Small molecules organic semiconductors (SMOS) possess distinct advantages compared with CPs, such as well-defined chemical structures with tunable structures, easy purification, good solubility, and no batch-to-batch variations. Owing to these unique properties, SMOS have been widely explored in organic photovoltaics, organic light-emitting diodes (OLEDs), solar cells, and organic thin-film transistors.[8-13] However, their use in photocatalytic applications is still rare. A recent work reported that conjugated thiophene-based trimers (Th-BT-Th) with donor-acceptor-donor (D-A-D) units can potentially be used for photocatalytic intermolecular C-H functionalization under visible light irradiation. The efficiency of Th-BT-Th was comparable to the state-of-art transition metal-based photocatalysts, such as $[Ru(bpy)_3]Cl_2$.[14] Therefore, this work opened the door for a new class of metal-free and visible light-active catalysts, based on small molecule organic semiconductors, for photochemical organic reactions. Besides, C. M. Aitchison *et al*. reported that different oligomers with D-D, A-A, D-A-D, and A-A-A present comparable photocatalytic H_2 production rates to the corresponding polymer. Thus, it demonstrated that high molar masses are not required for displaying high activity, while backbone planarity, bridgehead atom, and chain length have a greater impact on the photocatalytic property.[15] Despite the superior advantages of SMOS compared to CPs and inorganic semiconductors, they require prior dissolution in organic solvents before the photocatalytic reaction, which complicates their overall recovery and reusability.[16, 17]. Moreover, not all the powder dispersion, especially organic semiconductors, is equally exposed to the incident solar light due to the aggregation of powder and the limitations of the reactor design.

The merging of photocatalysis with cutting-edge technologies, such as three-dimensional (3D) printing, enables the design of supported photocatalysts with multiple shapes and versatile structures. Different 3D-printed photocatalysts have been reported, showing excellent photocatalytic activities for the degradation of organic pollutants and hydrogen generation.[18-22] The improved photocatalytic activity has been mainly attributed to better light harvesting by the hierarchical structure and the high surface area associated with the porous photocatalytic network. Therefore, 3D printing facilitates the

manufacturing of photoactive materials to develop robust photocatalytic systems with easy reusability without requiring any additional filtering.[20, 23-25]

Up to date, inorganic semiconductors have been mainly used for designing 3D-printed photocatalysts with applications in energy and environmental remediation.[26] However, the lack of solubility of such materials in organic solvents results in an inhomogeneous dispersion of the photocatalytic nanoparticles in the thermoplastics that complicates the whole fabrication and extrusion process. Here, we present, for the first time, the design of a 3D-printed hierarchical porous structure, containing an organic photoactive molecule, based on a conjugated trimer with a D-A-D configuration (EBE), for the photocatalytic degradation of persistent organic pollutants and hydrogen generation. Because of the high solubility of the EBE molecule in organic solvents, the resulting filaments showed good malleability and homogeneity similar to the ones without photocatalysts. The characterization of the 3D-printed structure showed that the photophysical and chemical properties of the organic semiconductor were maintained upon the 3D printing processing. Moreover, despite the low amount of the photocatalyst (0.05 %), the 3D-printed EBE (EBE-3D) structure showed good photocatalytic efficiencies for the removal of methylene blue and 4-nitrophenol pollutants and hydrogen generation under sun-like irradiation. Therefore, this work opens new horizons for practical photocatalytic applications of 3D-printed organic semiconductors in the fields of environmental remediation and solar fuels.

EXPERIMENTAL SECTION

Reagents. 4,7-Dibromo-2,1,3-benzothiadiazole (95%), potassium carbonate (K_2CO_3, ≥99.99%), PEPPSI^{TM}-IPr (98%), toluene (anhydrous, 99.8%), methanol (anhydrous, 99.8%), were purchased from Sigma-Aldrich and 3,4-Ethylenedioxythiophene-2-boronic acid pinacol ester was purchased from TCl. All the reagents were used as received. Deionized water (Milli-Q, 18.6 MΩ) was used throughout all experiments.

Synthesis of EBE. EBE was synthesized via a Suzuki coupling reaction. Briefly, 4,7-Dibromo-2,1,3-benzothiadiazole (400 mg) and 3,4-Ethylenedioxythiophene-2-boronic acid pinacol ester (800 mg) were dissolved in toluene/methanol (120:160 ml) in a flame-dried round-bottom flask. Argon was bubbled for 15 minutes in the solution to deaerate it. Then, K_2CO_3 (1.2 g) was added to the reaction in one portion and the mixture was heated to 40°C and stirred for 10 min. Then PEPPSI^{TM}-IPr catalyst (46 mg) was added under argon flow and the flask was sealed. The temperature was increased to 75°C

and the mixture was stirred for 4h. The reaction mixture was filtered, and the solid precipitate was washed with toluene and methanol and dried under a vacuum (**Figure S1**). ^{1}H NMR (400 MHz, DMSO-d6) δ 8.42 (s, 2H), 6.87 (s, 2H), 4.45 – 4.29 (m, 8H). ^{13}C NMR (400 MHz, DMSO-d6) δ 151.89, 142.04, 141.19, 126.39, 123.51, 112.58, 103.07, 65.55, 64.50.

3D printing of the EBE molecule. The 3D EBE structure was fabricated by fused deposition modeling (FDM), due to its low cost and good materials compatibility. The initial step includes the fabrication of the filament by mixing the photocatalyst with melted thermoplastic pellets, followed by an extrusion/heating process. For this purpose, 30 g of acrylonitrile butadiene styrene (ABS, Smart materials pellets©) and 15 mg of EBE catalyst were dissolved in 120 mL of acetone. The solution was sonicated for 3h until a homogeneous mixture was obtained. Then, the ABS-EBE solution was heated at 80 ºC to evaporate the acetone and obtain a solid orange film. The film was cut into pieces to obtain ABS-EBE shavings to make the filament. A Felfil-Evo© extruder and Felfil-Spooler© were used to extrude the filament at 180 ºC with a 1.7 mm diameter. EBE catalyst was 3D-printed by using a Creality3D Ender 3 V2 3D Printer and the software Ultimaker Cura©. The 3D structure was designed with FreeCad© and Solid Works© software (**Figure S2**).

Characterization of the 3D-printed EBE structure and EBE powder. ^{1}H and ^{13}C NMR spectra were recorded at ambient temperature with a 400 MHz Bruker Avance Spectrometer with a 5 mm BBFO probe in the appropriate deuterated solvent. The contents of residual Pd in trimers were measured by inductively coupled plasma-mass spectrometry (ICP-MS). The morphology of the EBE-3D was investigated by scanning electron microscope Quanta 600 FEI (Thermofisher) and the EDX detector from Oxford instruments. Absorption spectra were collected by using a UV-vis spectrometer (Agilent Cary 60) with a wavelength range of 350~800 nm. Fluorimeter (Fluorolog-QM, Horiba) was used to measure the emission fluorescence spectra and the lifetime of the samples was detected by the Lifetime TCSPC configuration, under excitation from a NanoLED. The pulse (instrument response) was determined by measuring the light scatted by a Ludox suspension. The lifetime was calculated by fitting the decays with a monoexponential model: $I(t) = I_0 * e^{-\frac{t}{\tau}}$, where t is the time and I_0 is the intensity at time zero. FTIR-ATR TR0 was used to investigate the functional groups present in the 3D-printed EBE sample. Raman spectra were collected by using an FTIR-FTRaman Thermo Nicolet iS50. X-ray diffraction (XRD) spectra of 3D EBE structure and EBE-pellet were obtained with a Bruker AXS D8-Discover diffractometer (40 kV and 40mA). Thermal analysis was conducted by using the Thermogravimetric balance (Mettler Toledo, TGA/SDTA851). X-ray photoelectron spectroscopy

(XPS) experiments were performed in a PHI 5500 Multitechnique System (from Physical Electronics) with a monochromatic X-ray source (Aluminium Kalfa line of 1486.6 eV energy and 350 W), placed perpendicular to the analyzer axis and calibrated using the $3d_{5/2}$ line of Ag with a full width at half maximum (FWHM) of 0.8 eV.

Photocatalytic Test. The photocatalytic activity of the 3D-printed EBE structure was assessed for the degradation of organic pollutants and the generation of hydrogen. For this purpose, methylene blue (MB, 50 ppm) and 4-nitrophenol (4-NP, 50 ppm) were used as model pollutants. Before irradiation, the 3D-printed EBE catalyst was placed in the respective pollutant solution and kept in dark for 30 minutes to ensure adsorption-desorption equilibrium. Specifically, for the photocatalytic degradation, the 3D-printed EBE cube was placed inside 25 mL of MB or 4-NP solutions under sun-like light irradiation (Ultra-vitalux 230V 300W, OSRAM). Then, 1 mL of an MB or 4-NP solution was taken out every 30 min and 1 hour, respectively. UV-vis spectrometer was used to record the absorption of pollutants. The degradation rate of pollutants is expressed as $(C_0\text{-}C)/C_0$ *100% (C_0-initial concentration; C-the concentration of taken samples). For hydrogen production, the 3D-printed catalyst was placed in 20 mL of N_2 degassed (30 min) aqueous solution with 25 vol% of methanol as a hole scavenger (the total volume of the reactor was 50 mL). The sample was exposed under solar simulator (AM1.5) irradiation. Before turning on the light, the reactor was degassed by flowing N_2 for 1h to remove the O_2 in the system. A single-quadrupole mass spectrometry (MS, Omnistar^{TM} GSD 320) connected to the reactor outlet was used to determine the amount of hydrogen generated online.

Evaluation of the generation of radicals. The photogenerated hydroxyl radicals ($HO^{\bullet}$) by EBE-3D structure was examined by using terephthalic acid (THA) as probe molecule. EBE-3D in THA (0.125 mM) solution was irradiated under sun-like light irradiation and then, 2 mL of solution was taken at 30 min, 1h and 2h, respectively. The fluorescence intensity of these solutions was obtained by Fluorimeter (Fluorolog-QM, Horiba). In addition, the photocatalytic activity of EBE-3D for MB decomposition was evaluated in the presence of different radical scavengers: 0.1M 2-propanol (0.5 mL, hydroxyl radical scavenger) and 0.1 M benzoquinone (0.5mL, superoxide radical scavenger).

RESULTS AND DISCUSSION

The conjugated trimer molecule (EBE) was synthesized by Pd (0)-catalyzed Suzuki-Miyaura cross-coupling reactions. The ^{1}H HMR and ^{13}C NMR characterizations are described in the Supporting Information, SI (**Figure S3-S4**). Here, 3,4-ethylenedioxythiophene (E) is used as a donor group due to its strong electron-donor properties with self-organization ability associated with non-covalent sulfur-oxygen interactions.[27] Benzothiadiazole (B) is a classical electron-deficient acceptor unit that is widely

used in polymer solar cells.[28] The preparation process of EBE-3D is shown in **Figure 1** and the 3D printing settings are specified in **Table S1**. It involves the melting of ABS pellets in combination with EBE in acetone. The resulting suspension was maintained at 80 ºC until a homogeneous mixture was obtained, followed by solvent evaporation (Figure 1a). The obtained orange thin film was cut into pieces and extruded to create the starting filaments (**Figure 1b**),

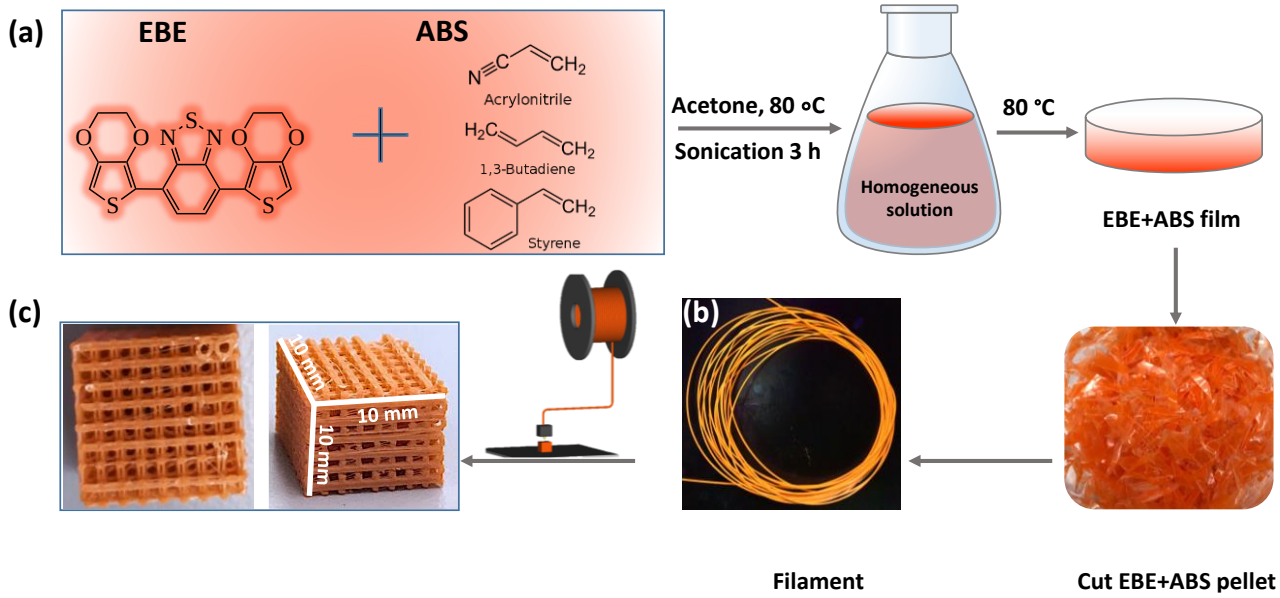

Figure 1. Schematic process for the fabrication of EBE-3D structures. (**a**) chemical structures of the EBE and ABS; (**b**) Filament of EBE-ABS; (**c**) EBE-3D.

Then, the EBE-based filament was 3D-printed in a cube morphology with an intertwined porous network of 0.5 mm diameter and a layer thickness of 0.2 mm. The resulting 3D-printed cubic structure has an overall width of 10 mm and a total height of 10 mm (**Figure S2**). SEM images show the left side view (**Figure 2a-c**) and top side view of the 3D-printed EBE catalyst (**Figure 2d-e**), which presents a homogenous and rough surface. The chemical composition of the 3D-printed catalyst was determined by EDS and the elemental mapping images and spectrum show the distributions of C, S, O elements, which corroborates the presence of EBE on the resulting 3D-printed structure (**Figure 2f-j**).

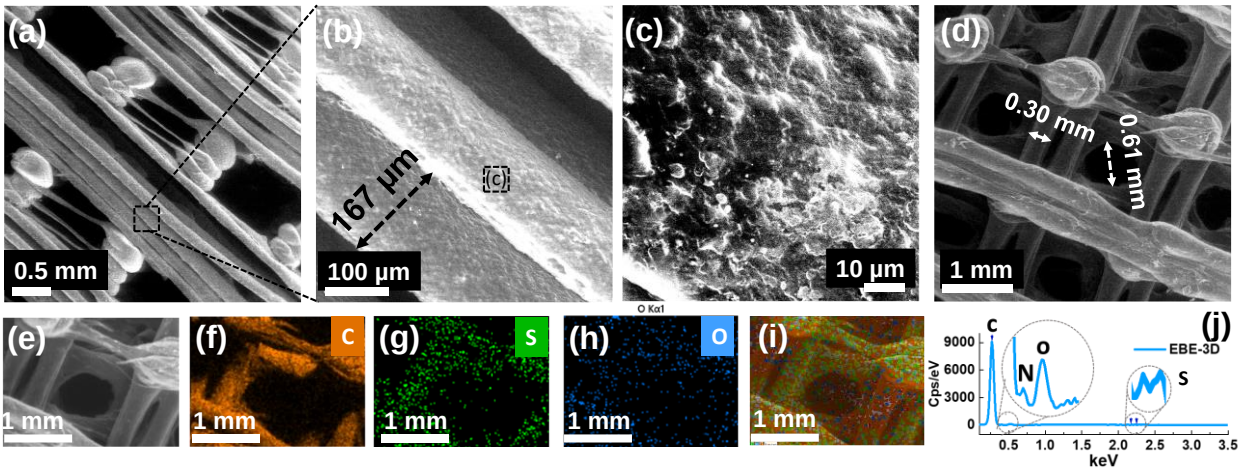

Figure 2. Morphological characterization of the 3D-printed EBE catalyst. (**a-c**) left side view of the EBE-3D; (**d-e**) top side view of the EBE-3D; EDS element mapping of C (**f**), S (**g**) and O (**h**) and C+S (**i**) and spectrum of EBE-3D (**j**).

For potential real-world photocatalytic applications, it is necessary to develop visible-light responsive materials that enable a strong solar light absorption capacity and high efficiencies. **Figure 3a** shows the normalized UV-vis absorption and emission spectra of the 3D-printed catalyst. It presents a strong absorption in the visible range, from 400 nm to 600 nm, with a maximum absorption band at λ_{max} = 486 nm and a strong orange fluorescence at λ_{ex} = 486 nm (~601 nm), which are consistent with the optical properties of EBE-powder (**Figure S5**). The Stokes shift (ca. 115 nm) suggests intramolecular charge transfer character in the single excited state of the 3D-printed EBE catalyst. Moreover, a single exponential function decay model of EBE powder and EBE-3D are exhibited in **Figure 3b**. Both EBE-powder and EBE-3D present long-lived emission decay on ns time scales. The average emissive lifetimes of the EBE-powder and EBE-3D are 1.4 ns and 11.7 ns, respectively. The relatively longer lifetime shown by the 3D-printed EBE structure in comparison with the EBE powder might be attributed to the microenvironment effect of solvent (acetone) and a strong intermolecular π-π stacking which effectively quench the fluorescence in the powder state.[29] Such a long lifetime of the photogenerated charge carriers allows electron-hole pairs to have more opportunities to participate in photocatalytic redox reactions before recombination.[30, 31] These results imply that 3D printing of organic small molecules is an efficient way to extend the lifetime of charge carriers in comparison to the solid powder state.

The FTIR spectrum of the 3D structure evidence the presence of small peaks of C-O-C (1158 cm^{-1}), C-O (1026 cm^{-1}), and C-S (750 cm^{-1}), which corresponds to the structure of the EBE organic molecule. A strong C≡N stretching band at 2237 cm^{-1} is assigned to the acrylonitrile (**Figure 3c**). The Raman spectra of samples are shown in **Figure S6**. Characteristic ABS bands appear in both spectra

of EBE-pellet (EBE film before extrusion) and EBE-3D. The peak located at ~1000 cm^{-1} is ascribed to the C-H (R-CH-CH_2) vinyl groups of polyacrylonitrile and polybutadiene. The small peaks from EBE can be also observed in EBE-pellet and EBE-3D. There is not much difference between EBE-pellet and EBE-3D, which suggests that 3D printing EBE does not alter the chemical composition of the EBE.

The thermal property of EBE-based samples was studied by the thermogravimetric analysis (TGA). EBE-3D shows good thermal stability with a decomposition temperature (100% weight loss) of 490 °C in nitrogen, which exhibits better thermal stability than EBE-powder (65% weight loss at 383 °C) (**Figure 3d**). This thermal enhancement might be related to the presence of the ABS polymer on the 3D-printed structure. XRD patterns of EBE-powder, EBE-pellet, EBE-3D are displayed in Figure S7. The broad peak at $2\theta = 20^{\circ}$ is attributed to ABS. Due to the low content of EBE, we could not observe distinct EBE characteristic peaks in EBE-pellet and/or EBE-3D (**Figure S7**). XPS survey spectra of the samples indicate the presence of C, N, O elements. Pd was only observed in EBE-powder, while in EBE-3D, there is no signal peaks of Pd, mainly because the content of EBE is too low compared to ABS in the EBE-3D sample (**Figure 3e**). Two sets of Pd 3d XPS peaks can be assigned to metallic Pd^0 (**Figure S8**). The high-resolution C 1s spectra of EBE-3D are shown in **Figure 3f**. The peaks centered at 284.5 eV and 286.1 eV are assigned to C-H/C-C/C=C and C=N/C-O from ABS, respectively. The small peak located at 285.4 eV is attributed to O-C=O from EBE, which also indicates the small amount of EBE in EBE-3D.[32-34]

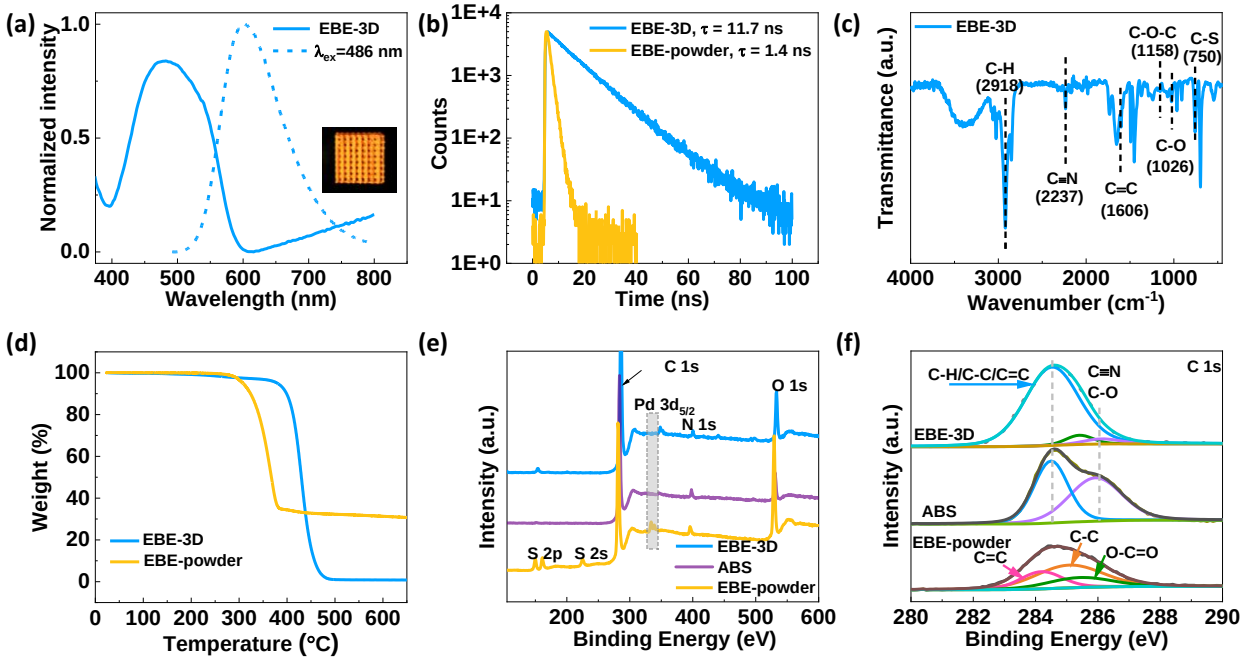

Figure 3. Characterization of EBE-based photocatalytic samples. (**a**) Normalized UV-vis spectra (solid line) and emission spectra (dash line) of and EBE-3D (inset image: EBE-3D under λ = 365 nm irradiation); (**b**) Fluorescence lifetime of EBE-powder and EBE-3D; (**c**) FTIR of and EBE-3D; (**d**) TGA of EBE-powder and EBE-3D; XPS spectra of (**e**) The survey spectra of the samples. (**f**) C 1s in EBE-powder, ABS, and EBE-3D.

Photocatalytic applications

The photocatalytic process mainly includes the light absorption, combination and separation of photogenerated carriers, and the redox reactions on the catalyst surface with the participation of excitons. The photocatalytic performance of EBE-3D with only 0.05% catalyst content (mass ratio EBE/ABS = 0.05%) was investigated by degradation of organic pollutant methylene blue (initial concentration C_0 = 50 ppm) and 4-nitrophenol (C_0 = 50 ppm) and hydrogen generation from water. As shown in **Figure 4a**, the degradation removal efficiency of MB is about 65% after 3h of sun-like light irradiation. The semi-logarithmic plot indicates the photocatalytic degradation of MB confirms to the first-order kinetic model (**Figure S9**). 4-NP presents a strong characteristic peak at 317 nm along with a weak peak at 400 nm (**Figure 4b**). In the presence of catalyst EBE-3D, the intensity of peaks of 4-NP reduced with temporal evolution. The degradation rate of 4-NP is around 27% after 3h and the regression curve of the nature logarithm of concentration versus time is also linear, suggesting the degradation of 4-NP over EBE-3D can be described as a first-order kinetic model (**Figure S10**). The stability of the EBE-3D is obtained through cyclic testing. After 5 cycles, the degradation rate of MB was maintained, which indicates the good stability of our EBE-3D catalyst (**Figure 4c and Figure S11**). In addition, the photocatalytic activity of cut EBE pellet were compared with EBE-3D, which showed lower activity for MB and 4-NP degradation (**Figure S12**).

Hydrogen is a clean and environmentally friendly source to solve the energy crisis and environmental contamination. Photocatalytic hydrogen generation through a water-splitting process has attracted much attention. Therefore, the performance of EBE-3D for photocatalytic hydrogen production was also investigated in a methanol-water solution. Methanol was used as a hole scavenger that reacts with the holes to produce CO_2 ($CH_3OH \rightarrow HCHO \rightarrow HCOOH \rightarrow CO_2$) [35] (insert figure in Figure 4d). To determine the H_2 is from photocatalytic reaction, additional controlled experiments were carried out including i) performing the photocatalysis in the absence of an EBE-3D catalyst and ii) under dark conditions. No H_2 was detected under both conditions suggesting the H_2 is produced by photocatalytic reduction reaction. As shown in **Figure 4d**, hydrogen production is increasing with time. After 7 h of reaction, the rate of hydrogen production was 5.4 μmol min^{-1}.

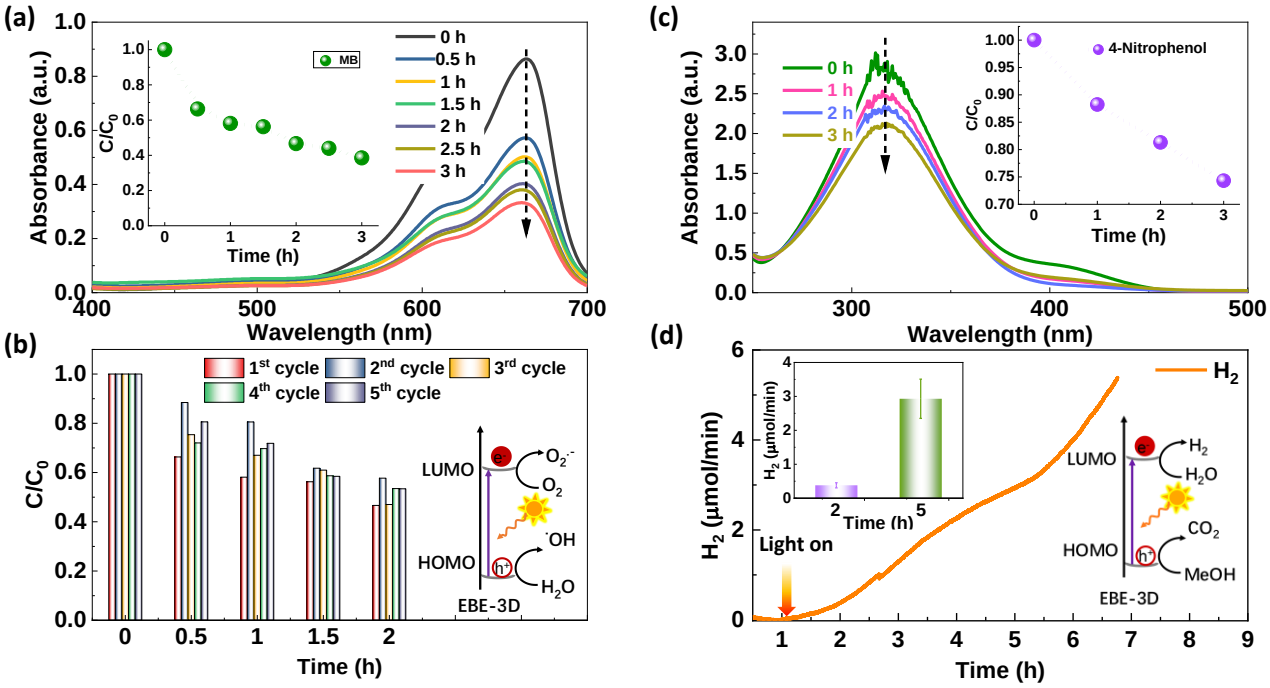

Figure 4. Photocatalytic performance of 3D-printed EBE catalyst for degradation of organic pollutants and hydrogen generation. (**a**) UV-vis absorption spectra of methylene blue and the degradation rate (insert figure) of EBE-3D; (**b**) The degradation rate of MB after 5 cycles of reuse and the proposed photocatalytic mechanism for the degradation (insert figure); (**c**) UV-vis absorption spectra of 4-nitrophenol and the degradation rate (insert figure) of EBE-3D; (**d**) Time courses of hydrogen evolution from methanol/H_2O (vol.% = 1:3) solution and proposed photocatalytic mechanism for hydrogen production (insert figure) and upper insert image shows the activity at 2 h and 5 h, respectively.

During photocatalytic process, the photogenerated electron-hole pairs react with the adsorbed molecules to generate various redox free radicals, which will further oxidize organic pollutants into CO_2 and water. Among these active free radicals, hydroxyl radicals (˙OH) and superoxide radicals ($O_2^{\cdot-}$) are considered to play a crucial role in photocatalytic efficiency. To further prove the effect of photogenerated ˙OH ($H_2O + h^+ \rightarrow {}^{\cdot}OH$) and $O_2^{\cdot-}$ ($O_2 + e^- \rightarrow O_2^{\cdot-}$) on the oxidation of organic pollutants (such as MB and 4-NP) (insert figure in Figure 4b). Hydroxylation of aromatic compounds has been used to detect hydroxyl radicals. Terephthalate (THA) is a particularly sensitive probe of ˙OH.[36] Due to the symmetry of THA (non-fluorescent), only one monohydroxylate isomer (THA-OH, fluorescent) is produced when reacting with hydroxyl radicals (see **Figure5b**). **Figure 5a** shows the increase in fluorescent intensity of THA-OH as a function of time, which indicates that ˙OH radicals are generated as the photocatalytic reaction proceeds. When 2-propanol (as a ˙OH scavenger) was added to the photocatalytic reaction, the degradation rate of MB was significantly decreased, while when

benzoquinone (as superoxide radical scavenger) was added, the activity was close to that without adding any sacrificial agent (**Figure 5c-d**). These results suggested that the photocatalytic degradation of MB by 3D-EBE is mainly caused by ˙OH radicals.

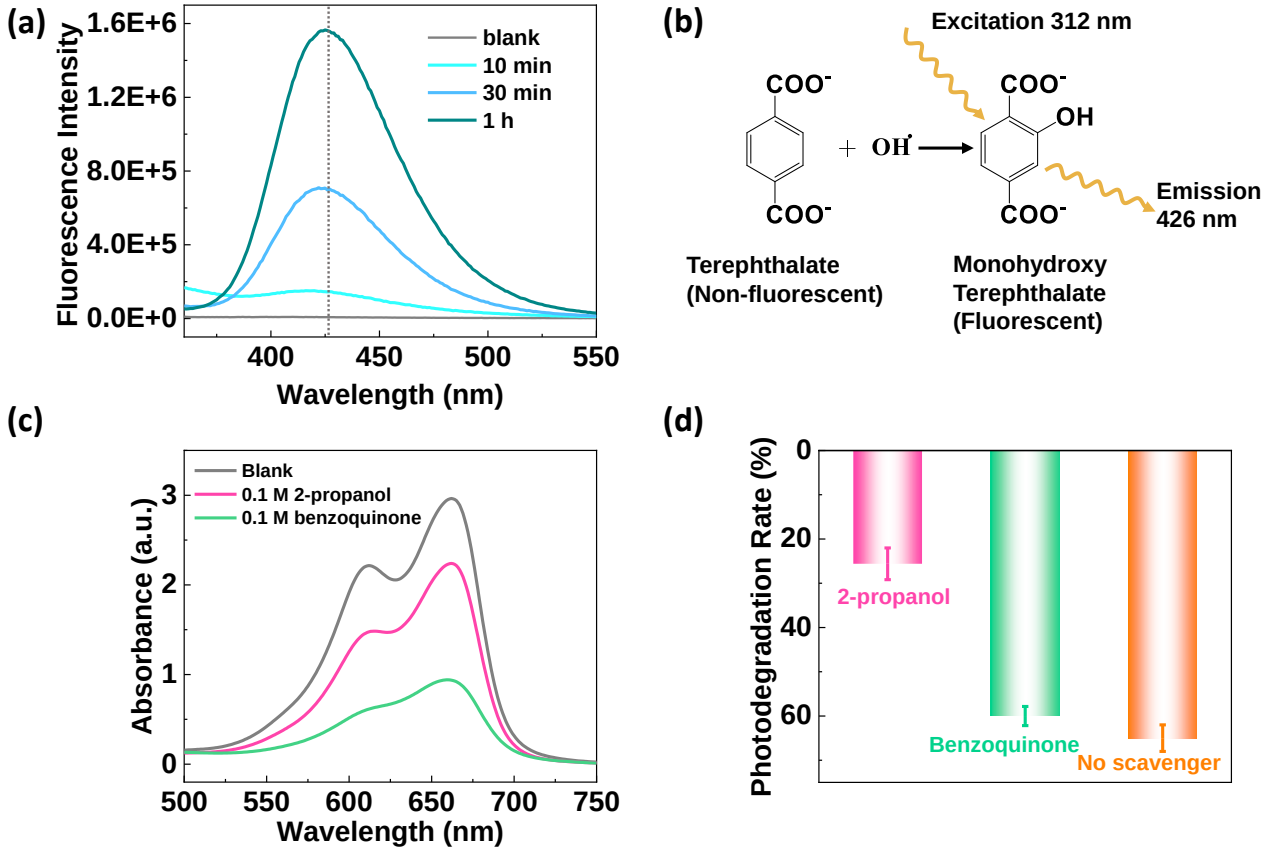

Figure 5. (**a**) Fluorescence spectra of THA-OH with the evolution of photocatalytic reaction time; (**b**)Hydroxyl radicals react with THA to yield fluorescent THA-OH; (**c**) UV-Vis absorption of MB in the presence EBE-3D with additional 0.1 M 2-propanol and 0.1 M benzoquinone after 3 h sun-like lamp irradiation; (**d**) Photodegradation rate of MB in the presence of different scavengers.

A comparison of the photocatalytic performance of main 3D-printed photocatalysts reported in the literature is included in **Table 1**. The photocatalyst catalyst content (0.05%) present in the 3D-printed EBE structure is the lowest reported so far. Moreover, compared to 3D-printed inorganic photocatalysts, our system showed better photocatalytic performances for pollutant removal and hydrogen generation under visible light irradiation. For instance, the photogenerated H_2 rate by our 3D-printed EBE photocatalyst was 2x higher (5.4 µmol min^{-1}) than that obtained with TiO_2/Au (2.2 µmol min^{-1}). Therefore, these results demonstrate the potential of 3D-printed EBE-based molecule for potential scalable photocatalytic processes under solar light irradiation.

Table 1. A comparison of 3D-printed photocatalysts for MB degradation and hydrogen generation

3D-printing Samples	Mass Ratio (Catalysts ratio)	Light source	Degradation rate (MB)	H_2 production	Ref.
LDPE-TiO_2	1%	UV (300-380 nm)	14% (2h)	-	[19]
ZnO-NF	50%: 50%	UV-Vis	100% (2h)	-	[20]
Au/TiO_2	66%	UV LEDs (λ = 365±5 nm)	-	2.2 μmol min^{-1}	[21]
Al_2O_3/TiO_2/Pt/C3DP	65%	UV-Vis (500 W Xe/Hg lamp)	-	101 μmol g^{-1} h^{-1}	[22]
TNT (857 μm)	50%	UV LEDs (λ = 365±5 nm)	K=0.0501 min^{-1}	-	[24]
EBE-3D	0.05%	UV-Vis (300 W Xe lamp)	65% (3h)	5.4 μmol min^{-1}	This work

CONCLUSIONS

In summary, an organic conjugated small molecule, EBE trimer, was successfully 3D-printed for the first time. The excellent solubility of the EBE trimer in organic solvents facilitated the whole extrusion and 3D printing process, resulting in resistant photocatalytic-based filaments similar to bare thermoplastics. Interestingly, the 3D-printed EBE structure exhibited a longer lifetime of photogenerated carriers in comparison to EBE in a powder state due to the microenvironmental effect from the solvent and the less aggregation of EBE compare with EBE-powder. As a proof-of-concept, the photocatalytic performance of EBE-3D was investigated for the degradation of organic pollutants (MB and 4-NP) and hydrogen production, showing competitive photocatalytic rates under sun-like irradiation with only 0.05% catalyst content. Moreover, the stability of the 3D-printed photocatalyst was demonstrated up to 5 cycles. Therefore, this work opens new avenues for the fabrication of immobilized organic small molecules by 3D printing technology, enabling the design of hierarchical and porous structures with high efficiencies in the fields of environmental remediation and energy applications.

ASSOCIATED CONTENT

Supporting Information.

The Supporting Information is available free of charge on the Wiley Publications website.

Additional results on 3D design details; ^{1}H and ^{13}C NMR spectrum; Absorption spectrum and emission spectra of EBE dissolved in acetone; Raman spectra; XRD spectra; Survey spectra of the samples; Kinetic plot for the photodegradation of MB and 4-NP; UV-vis absorption spectra of MB for photocatalytic cycle test. (PDF)

AUTHOR INFORMATION

Corresponding Author

*Katherine Villa. Institute of Chemical Research of Catalonia (ICIQ), The Barcelona Institute of Science and Technology (BIST). Av. Països Catalans, 16, Tarragona E-43007, Spain. orcid.org/0000-0003-1917-0299. Email: kvilla@iciq.es.

Author Contributions

The manuscript was written through contributions of all authors. All authors have given approval to the final version of the manuscript.

Notes

The authors declare no competing financial interest.

ACKNOWLEDGMENT

X.Y. and K. V. acknowledges the support from the “la Caixa” Foundation (ID 100010434) with the fellowship code LCF/BQ/PI21/11830017.

REFERENCE

1. C. Dai and B. Liu, *Energy & Environmental Science*, 2020, **13**, 24-52.
2. G. Zhang, Z. A. Lan and X. Wang, *Angewandte Chemie International Edition*, 2016, **55**, 15712-15727.
3. C. Zhao, Z. Chen, R. Shi, X. Yang and T. Zhang, *Advanced Materials*, 2020, **32**, 1907296.
4. R. S. Sprick, B. Bonillo, R. Clowes, P. Guiglion, N. J. Brownbill, B. J. Slater, F. Blanc, M. A. Zwijnenburg, D. J. Adams and A. I. Cooper, *Angewandte Chemie International Edition*, 2016, **55**, 1792-1796.
5. X. Yuan, C. Wang, D. Dragoe, P. Beaunier, C. Colbeau-Justin and H. Remita, *Applied Catalysis B: Environmental*, 2021, **281**, 119457.
6. J. Li, X. Gao, L. Zhu, M. N. Ghazzal, J. Zhang, C.-H. Tung and L.-Z. Wu, *Energy & Environmental Science*, 2020, **13**, 1326-1346.

7. X. Yuan, D. Dragoe, P. Beaunier, D. B. Uribe, L. Ramos, M. G. Méndez-Medrano and H. Remita, *Journal of Materials Chemistry A*, 2020, **8**, 268-277.
8. A. Mishra and P. Bäuerle, *Angewandte Chemie International Edition*, 2012, **51**, 2020-2067.
9. Y. Lin, Y. Li and X. Zhan, *Chemical Society Reviews*, 2012, **41**, 4245-4272.
10. D. Gedefaw, M. Prosa, M. Bolognesi, M. Seri and M. R. Andersson, *Advanced Energy Materials*, 2017, **7**, 1700575.
11. S.-H. Kang, D. Lee, H. Kim, W. Choi, J. Oh, J. H. Oh and C. Yang, *ACS Applied Materials & Interfaces*, 2021, **13**, 52840-52849.
12. Y. Zheng, S. Bao, H. Yang, H. Fan, D. Fan, C. Cui and Y. Li, *Chemical Communications*, 2021, **57**, 10767-10770.
13. A. Can, G.-S. Choi, R. Ozdemir, S. Park, J. S. Park, Y. Lee, I. b. Deneme, E. Mutlugun, C. Kim and B. J. Kim, *ACS Applied Polymer Materials*, 2022, **4**, 1991-2005.
14. L. Wang, W. Huang, R. Li, D. Gehrig, P. W. Blom, K. Landfester and K. A. Zhang, *Angewandte Chemie International Edition*, 2016, **55**, 9783-9787.
15. C. M. Aitchison, M. Sachs, M. A. Little, L. Wilbraham, N. J. Brownbill, C. M. Kane, F. Blanc, M. A. Zwijnenburg, J. R. Durrant and R. S. Sprick, *Chemical Science*, 2020, **11**, 8744-8756.
16. J. Tang, J. Wang, L. Tang, C. Feng, X. Zhu, Y. Yi, H. Feng, J. Yu and X. Ren, *Chemical Engineering Journal*, 2022, **430**, 132669.
17. Z. Ma, P. Zhou, L. Zhang, Y. Zhong, X. Sui, B. Wang, Y. Ma, X. Feng, H. Xu and Z. Mao, *Cellulose*, 2021, **28**, 3531-3547.
18. K. Li, Y. de Rancourt de Mimérand, X. Jin, J. Yi and J. Guo, *ACS Applied Nano Materials*, 2020, **3**, 2830-2845.
19. M. J. M. de Vidales, A. Nieto-Márquez, D. Morcuende, E. Atanes, F. Blaya, E. Soriano and F. Fernández-Martínez, *Catalysis Today*, 2019, **328**, 157-163.
20. S. Son, P.-H. Jung, J. Park, D. Chae, D. Huh, M. Byun, S. Ju and H. Lee, *Nanoscale*, 2018, **10**, 21696-21702.
21. A. Elkoro, L. Soler, J. Llorca and I. Casanova, *Applied Materials Today*, 2019, **16**, 265-272.
22. M. Z. Hussain, P. F. Großmann, F. Kohler, T. Kratky, L. Kronthaler, B. van der Linden, K. Rodewald, B. Rieger, R. A. Fischer and Y. Xia, *Solar RRL*, 2022, 2200552.
23. W. Guo, Y. Liu, Y. Sun, Y. Wang, W. Qin, B. Zhao, Z. Liang and L. Jiang, *Advanced Functional Materials*, 2021, **31**, 2100768.
24. H. Sopha, A. Kashimbetova, L. Hromadko, I. Saldan, L. Celko, E. B. Montufar and J. M. Macak, *Nano Letters*, 2021, **21**, 8701-8706.
25. N. Fijoł, H. N. Abdelhamid, B. Pillai, S. A. Hall, N. Thomas and A. P. Mathew, *RSC advances*, 2021, **11**, 32408-32418.
26. J. Muñoz, D. Rojas and M. Pumera, *ACS Applied Energy Materials*, 2022, **5**, 3252-3258.
27. D. Demeter, T. Rousseau and J. Roncali, *RSC advances*, 2013, **3**, 704-707.
28. P. Zhou, Z.-G. Zhang, Y. Li, X. Chen and J. Qin, *Chemistry of Materials*, 2014, **26**, 3495-3501.
29. K. Shirai, M. Matsuoka and K. Fukunishi, *Dyes and pigments*, 1999, **42**, 95-101.
30. P. Yang, Y. Zhang, H. Zhang, J. Zhao, Z. Wei, H. Shi, Z. Zheng, Y. Huang and H. Yang, *ACS Catalysis*, 2022, **12**, 6276-6284.
31. Y. Wang, X. Shang, J. Shen, Z. Zhang, D. Wang, J. Lin, J. Wu, X. Fu, X. Wang and C. Li, *Nature communications*, 2020, **11**, 1-11.
32. N. H. N. Azman, M. S. Mamat, H. N. Lim and Y. Sulaiman, *Journal of Materials Science: Materials in Electronics*, 2018, **29**, 6916-6923.
33. F.-P. Du, N.-N. Cao, Y.-F. Zhang, P. Fu, Y.-G. Wu, Z.-D. Lin, R. Shi, A. Amini and C. Cheng, *Scientific reports*, 2018, **8**, 1-12.
34. Z. Wang, Z. Li, Y. He and Z. Wang, *Journal of the Electrochemical Society*, 2011, **158**, D664.
35. J. Zhao, R. Shi, Z. Li, C. Zhou and T. Zhang, *Nano Select*, 2020, **1**, 12-29.

36. W. Freinbichler, M. A. Colivicchi, M. Fattori, C. Ballini, K. F. Tipton, W. Linert and L. Della Corte, *Journal of neurochemistry*, 2008, **105**, 738-749.